Comparison of DTC-C and DTC-SVM Applied in the Photovoltaic Water Pumping System

Chergui I.M[#1], Bourahla.M[*2],

Department of electrotechnics. University of Sciences and Technology of Oran
Laboratory of Electrical Drives and Power Electronics
BP 1505 Al Mnaouar, 31000 Oran, Algeria

[1]chergui_cum@yahoo.fr
[2]bourah3@yahoo.fr

***Abstract*— This paper deals the comparison of two different controls of Direct Torque applied on the induction motor. Direct Torque Control-classical and using space vector modulation associated to a photovoltaic water pumping system. Direct Torque Control (DTC) is based on instantaneous space vector theory, by optimal selection of the space voltage vectors in each sampling period, DTC collection effective control of the stator flux and torque. The most important advantage of this method is its rotor position free control system. In order to improve the efficiency of the photovoltaic energy generation, a maximum power point tracking with incremental conductance (Inc-MPPT) algorithm is applied under variable temperature and irradiance conditions. The system with DTC and integration of Inc-MPPT algorithm allows us to obtain a system operating at maximum power and functioning with a performance and fast response with no overshoot. We have optimized not only the efficiency of the photovoltaic conversion, but also, the losses in the induction motor and the optimization of the quantity of water flow.**

***Keywords*— Solar cell, Induction motor, Photovoltaic pumping system, Optimization, Inc-MPPT, Direct Torque Control.**

I. INTRODUCTION

The use of solar energy for different applications, mainly water pumping, is well suited to most of the scattered areas due to lack of electrification, the depth of the groundwater, the needs of drinking water and irrigation. The irradiation intensity is strongly fleet. The energy storage time is inevitable to match the change in energy demand. For electrical storage, the battery is used, but the size of the battery is too large compared with its capacity and it is not friendly to the environment. Strategy of storing water in a tank is more practical and economical than storing electricity in batteries. A solar cell is a solid state electrical device that converts the energy of visible light directly into continuous electricity by the photovoltaic effect. There are several types of technologies; each type has its peak power and efficiency.

To supply an induction motor (IM), we must use a better technique to control the inverter-IM and achieve an optimization of water flow pumping [2],[3]. We will formulate a comparison between the performances of the two controls techniques: conventional direct torque control (DTC-C) and using space vector modulation (DTC-SVM) in static and dynamic regimes. In steady state, and reference quantities for the current ripple and torque will be evaluated and compared for different values of speed and load. Transient, the expected object is to evaluate the method that gives the best dynamic response (speed without overshoot). This study is done for the criteria imposed almost the same switching frequency. The load and speed are nominal values. The implementation of the two commands has been really used with advanced microelectronics. Indeed, they require calculations transformed Park, evaluating trigonometric functions, integration and regulations. This could not be done in pure analogy. The methods of DTC-IM, competitive as conventional methods, are based on a feed pulse width modulation and a decoupling and motor flux orientation by the magnetic field torque. These controls have the same objective as the separately excited DC motor where the current and flux are naturally decoupled and can be controlled independently [3]-[8]. The comparison of the techniques is based on various criteria including the static and dynamic performance of the control feature basis. The study is conducted by simulation using Matlab/Simulink.

II. SOLAR CELL

An ideal solar cell (also called photovoltaic cell) may be modelled by a current source in parallel with a diode; in practice no solar cell is ideal, so a shunt resistance and a series resistance component are added to the model [2],[3]. The equivalent circuit of a solar cell is represented in Fig.1.

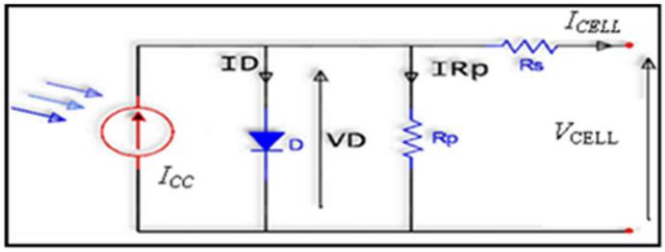

Fig.1 The equivalent circuit of a PV cell

From the equivalent circuit it is evident that the current produced by the solar cell is equal to that produced by the current source, minus that which flows through the diode, minus that which flows through the shunt resistor. The cell characteristic I = f (V) in the obscurity is presented as a diode on silicon (by the Shockley diode) as following:

$$I_{CELL} = I_D = I_{SAT}\left(\exp\left(\frac{V_{CELL}}{nV_T}\right)-1\right) \quad (1)$$

However, if the cell is under the illumination, the relationship becomes:

$$I_{CELL} = I_{CC} - I_D - I_{\mathrm{Rsh}} = I_{CC} - I_{SAT}\left(\exp\left(\frac{V_{CELL}}{nV_T}\right)-1\right) - I_{\mathrm{Rsh}} \quad (2)$$

The characteristic equation of a solar cell, which relates solarcell parameters to the output current and voltage:

$$I_{CELL} = I_{CC} - I_{SAT}\left(\exp\left(\frac{(V_{CELL}+R_S I_{CELL})}{nV_T}\right)-1\right) - \frac{V_{CELL}+R_S I_{CELL}}{R_{Sh}} \quad (3)$$

Where: I_D (A) diode current; I_{SAT} (A) reverse saturation current; I_{CELL}(A) output current; I_{RSh} (A) shunt current; V_{CELL}(V) voltage across the output terminals; I_{CC} (A) photogenerated current; n diode ideality factor; R_S/R_{Sh} (Ω), series/shunt resistance; V_T (V) thermodynamic potential.

In principle, given a particular operating voltage the equation may be solved to determine the operating current at that voltage. However, because the equation involves the current on both sides in a transcendental function the equation has no general analytical solution. However, even without a solution it is physically instructive. Furthermore, it is easily solved using numerical methods. Since the parameters I_{sat}, n, R_S, and R_{Sh} cannot be measured directly, the most common application of the characteristic equation is nonlinear regression to extract the values of these parameters on the basis of their combined effect on solar cell behavior.

When the cell is operated at open circuit, $I_{CELL} = 0$ and the voltage across the output terminals is defined as the open-circuit voltage. Assuming the shunt resistance is high enough to neglect the final term of the characteristic equation, the open-circuit voltage V_{OC} is:

$$V_{OC} \approx \frac{nkT}{q}\ln\left(\frac{I_{CC}}{I_{SAT}}+1\right) \quad (4)$$

When the cell is operated at short circuit, $V_{CELL} = 0$ and the current I_{CELL} through the terminals is defined as the short-circuit current. It can be shown that for a high-quality solar cell (low R_S and I_{SAT} and high R_{Sh}) the short-circuit current I_{SC} is equal to $I_{CELL.}$ It should be noted that it is not possible to extract any power from the device when operating at either open circuit or short circuit conditions. The values of I_{SAT}, R_S, and R_{SH} are dependent upon the physical size of the solar cell. In comparing otherwise identical cells, a cell with twice the surface area of another will, in principle, have double the I_{SAT} because it has twice the junction area across which current can leak. It will also have half the RS and RSH because it has twice the cross-sectional area through which current can flow,[2],[8]-[10]. For this reason, the characteristic equation is frequently written in terms of current density, or current produced per unit cell area:

$$J_{CELL} = J_{CC} - J_{SAT}\left(\exp\left(\frac{(V_{CELL}+r_S J_{CELL})}{nV_T}\right)-1\right) - \frac{V_{CELL}+r_S J_{CELL}}{r_{Sh}} \quad (5)$$

Where: J_{CELL} = current density (ampere/cm^2); J_{CC} = photogenerated current density (ampere/cm^2); J_{SAT} = reverse saturation current density (ampere/cm^2); r_S/r_{Sh} = specific series/shunt resistance (Ω-cm^2).

III. State representation of IM

Example of a state representation of IM a referential connected to the stator with θs = 0; follows: $X = [i_{s\alpha}\ i_{s\beta}\ \varphi_{r\alpha}\varphi_{r\beta}]$ of system dX/dt = AX+BU.

$$\begin{bmatrix} \frac{di_{s\alpha}}{dt} \\ \frac{di_{s\beta}}{dt} \\ \frac{d\varphi_{r\alpha}}{dt} \\ \frac{d\varphi_{r\beta}}{dt} \end{bmatrix} = \begin{bmatrix} -\left(\frac{R_s}{L_s\sigma}+\frac{(1-\sigma)}{T_r\sigma}\right) & 0 & \frac{(1-\sigma)}{T_r L_m\sigma} & \frac{(1-\sigma)}{L_m\sigma}p\omega \\ 0 & -\left(\frac{R_s}{L_s\sigma}+\frac{(1-\sigma)}{T_r\sigma}\right) & -\frac{(1-\sigma)}{L_m\sigma}p\omega & \frac{(1-\sigma)}{T_r L_m\sigma} \\ \frac{L_m}{T_r} & 0 & -\frac{1}{T_r} & -p\omega \\ 0 & \frac{Lm}{Tr} & p\omega & \frac{1}{T_r} \end{bmatrix} \cdot \begin{bmatrix} i_{s\alpha} \\ i_{s\beta} \\ \varphi_{r\alpha} \\ \varphi_{r\beta} \end{bmatrix} + \begin{bmatrix} \frac{1}{\sigma L_s} & 0 \\ 0 & \frac{1}{\sigma L_s} \\ 0 & 0 \\ 0 & 0 \end{bmatrix} \cdot \begin{bmatrix} V_{s\alpha} \\ V_{s\beta} \end{bmatrix} \quad (6)$$

IV. Factors affecting energy conversion efficiency

The maximum theoretically possible conversion efficiency for sunlight is 86% due to the Carnot limit, given the temperature of the photons emitted by the sun's surface [11]. However, solar cells operate as quantum energy conversion devices, and are therefore subject to the "thermodynamic efficiency limit". Photons with energy below the band gap of the absorber material cannot generate a hole-electron pair, and so their energy is not converted to useful output and only generates heat if absorbed. For photons with energy above the band gap energy, only a fraction of the energy above the band gap can be converted to useful output. When a photon of greater energy is absorbed, the excess energy above the band gap is converted to kinetic energy of the carrier combination. The excess kinetic energy is converted to heat through phonon interactions as the kinetic energy of the carriers slows to equilibrium velocity. Solar cells with multiple band gap absorber materials improve efficiency by dividing the solar spectrum into smaller bins where the thermodynamic efficiency limit is higher for each bin [12]. When a photon is absorbed by a solar cell it can produce an electron-hole pair. One of the carriers may reach the p-n junction and contribute to the current produced by the solar cell; such a carrier is said to be collected. Or, the carriers recombine with no net contribution to cell current. Quantum efficiency refers to the percentage of photons that are converted to electric current (i.e. collected carriers) when the cell is operated under short circuit conditions. The "external" quantum efficiency of a silicon solar cell includes the effect of optical losses such as transmission and reflection. However, it is often useful to look at the quantum efficiency of the light left after the reflected and transmitted light has been lost. "Internal" quantum efficiency refers to the efficiency with which photons that are not reflected or transmitted out of the cell can generate collectable carriers. Quantum efficiency is most usefully expressed as a spectral measurement (that is, as a function of photon wavelength or energy). Since some wavelengths are

absorbed more effectively than others, spectral measurements of quantum efficiency can yield valuable information about the quality of the semiconductor bulk and surfaces. Quantum efficiency alone is not the same as overall energy conversion efficiency, as it does not convey information about the fraction of power that is converted by the solar cell.

V. DIRECT TORQUE CONTROL OF IM

The basic principle of direct torque control based on the application of a particular sequence voltages via an inverter whose waves are generated through hysteresis comparators by which the flux and torque are trapped. The flux and torque are given by:

$$\overline{\varphi}_S = \int_0^t \left(\overline{v}_S - R_S.\overline{i}_S\right)dt \approx \Delta\overline{\varphi_s} = \overline{v_s}T_e \quad (7)$$

$$T_{em} = p\left(\varphi_{s\alpha} i_{s\beta} - \varphi_{s\beta} i_{s\alpha}\right) \quad (8)$$

$$\text{So } \frac{dT_{em}}{dt} = p\frac{M}{\sigma L_S L_r}.\varphi_S^* \varphi_r \omega_S \quad (9)$$

The estimated values of the flux and torque are compared to their prescribed values Φ_{sref}, T_{emref} respectively. Switching states are selected according to the table selector switch,[2],[4],[6]. The different switching table of DTC are shown in Table I.

TABLE.I
SWITCHING TABLE OF THE DTC.

$\Delta\varphi_s$	ΔT_{em}	1	2	3	4	5	6
1	1	V2	V3	V4	V5	V6	V1
	0	V7	V0	V7	V0	V7	V0
0	1	V3	V4	V5	V6	V1	V2
	0	V0	V7	V0	V7	V0	V7

Direct torque control of an IM is based on the "direct" determination of the control sequence applied to the switches of a voltage inverter. This choice is usually based on the use of hysteresis controllers whose function is to control the state of the system, namely here the amplitude of the stator flux and the electromagnetic torque. This type of strategy is therefore classified in the category of orders amplitude versus control laws and more traditional time-based adjustment of the average value of the voltage vector pulse width (PWM). The original DTC orders were strongly based on the "physical sense" and a relatively empirical approach to change states (flux, torque) on a very short interval of time [2]-[6].

VI. APPLICATION OF DTC-C IN A SOLAR PUMPING SYSTEM

The block diagram of the simulation is presented in Fig. 2. We present the various curves of the simulation of a control solar pumping system using DTC-C. This control method has the following advantages [13]-[16]:

Not require calculations in the rotor reference frame (d, q); there is no calculating block voltage modulation; it is not necessary to make a current decoupling relative to the control voltages; to have a single regulator, the outer loop speed; the dynamic response is very fast due to the absence of PI controller for the current in a rapid response of the pumping system. And disadvantages: The existence of the electromagnetic torque ripple; the existence of the ripples in the stator flux; the existence of a high bias currents; the switching frequency is variable (using hysteresis comparators).

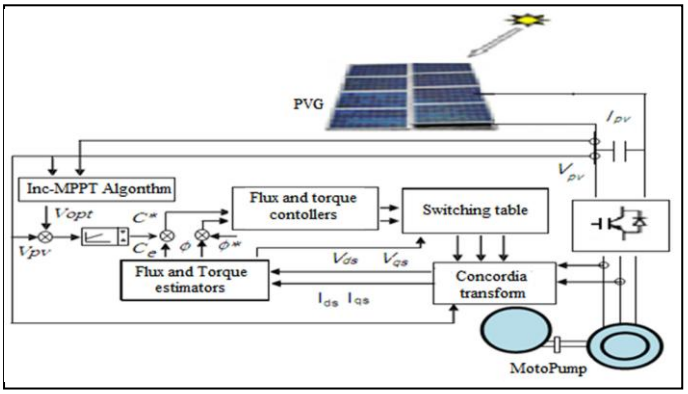

Fig.2 Block diagram of the DTC-C applied in the PV water pumping system.

VII. APPLICATION OF DIRECT TORQUE CONTROL USING SPACE VECTOR MODULATION (DTC-SVM)

This is a control method, developed as an alternative to the DTC-C. Its main feature is the elimination of hysteresis controllers and the selection table vectors, which eliminates the problems that were associated with it. In this control method, a vector PWM modulation is applied to the "vector increment desired stator flux" on the control output, where the input modulation algorithm components are obtained. The objective of this method is to make a direct stator flux vector control, a reference connected to the stator (α, β). Thus, we consider two flux vectors, the estimated stator flux vector and the reference. From these components, the increment desired stator flux vector at a given time is calculated [2],[6],[7]. The block diagram of the simulation of PV pumping system applied by the DTC-SVM is represented by Fig.3.

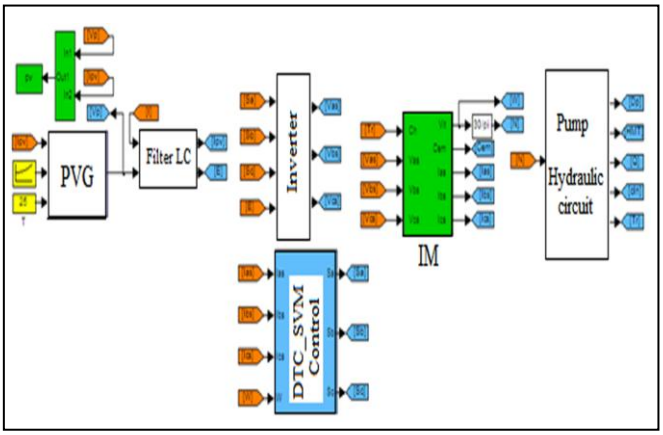

Fig. 3 Block diagram of the simulation of PV water pumping system applied by the DTC- SVM.

VIII. OPTIMIZATION OF PHOTOVOLTAIC SYSTEM

The power of the pump by PVG group is complemented by the inclusion of a mechanism for monitoring the maximum power combined with a classic proportional controller to improve performance. The optimization of PV pumping system is to maximize the amount of water pumped, which is to maximize the driving speed for each illumination, or performance PVG–IM.

To find the maximum power point (PPM) of PVG we need the derivative of the power delivered by PVG compared to the voltage. The ratio dP_{PVG}/dV_{PVG} is equal to zero, i.e.:

$$P_{PVG} = V_{PVG} \cdot I_{PVG} = (N_s \cdot V_{PV})(N_P \cdot I_{PV}) N_T V_{PV} \cdot I_{PV} \quad (10)$$

$$\text{So} \quad \frac{dP_{PVG}}{dV_{PVG}} = \frac{dI_{PVG}}{dV_{PVG}} \cdot V_{PVG} + I_{PVG} = 0 \quad (11)$$

To research a maximum point power, we can write:

$$\frac{dI_{MPP}}{dV_{MPP}} = -\frac{I_{OP}}{V_{OP}} \quad (12)$$

Note that the left-hand side of equation (12) represents the opposite of the PV array's instantaneous conductance, while the right-hand side represents its incremental conductance. Thus, at the Maximum Power Point, these two quantities must be equal in magnitude, but opposite in sign. If the operating point is off of the MPP, a set of inequalities can be derived from equation (12) that indicates whether the operating voltage is above or below the MPP voltage. These relationships are summarized as follow in equations (13)-(15).

$$\frac{dI_{MPP}}{dV_{MPP}} = -\frac{I_{OP}}{V_{OP}} \quad \text{IF} \quad \frac{dP_{PV}}{dV_{PV}} = 0 \quad (13)$$

$$\frac{dI_{MPP}}{dV_{MPP}} < -\frac{I_{OP}}{V_{OP}} \quad \text{IF} \quad \frac{dP_{PV}}{dV_{PV}} < 0 \quad (14)$$

$$\frac{dI_{MPP}}{dV_{MPP}} > -\frac{I_{OP}}{V_{OP}} \quad \text{IF} \quad \frac{dP_{PV}}{dV_{PV}} > 0 \quad (15)$$

For convenience, equation (13) is similar to equation (12). In turn, equations (14) and (15) are used to determine the direction in which a perturbation must occur to shift the operating point toward the MPP, and the perturbation is repeated until equation (13) is satisfied. Once the MPP is reached, the MPPT continues to operate at this point until a change in current is measured which will correlate to a change in irradiance on the array. For an optimal operating point, the PV array works at its maximum power and thus the derived power at this point is null. During the accurate tracking cycle, the PVG terminal voltage is adjusted by comparing the values of the incremental conductance and instantaneous one [17]-[19]. The following simulation will be presented taking into account: The technique of controlling the inverter; the insertion of the Inc-MPPT; the effect of changing weather conditions; as the target engine is installed in a PV pumping system, power supply mainly depends on solar radiation, so it is constantly changing. In this context, it is necessary that the power required is adjusted continuously with the production of energy from PVG. In what follows, we present the simulation results of the operation of solar pumping system using the MPPT with T= 25°C as is shown in Fig. 4.

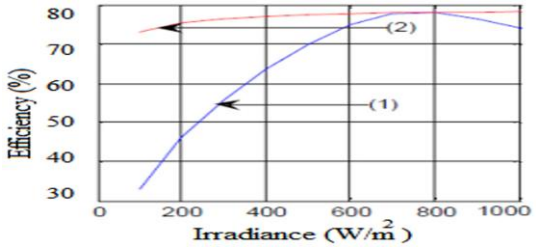

(1) Before optimization; (2) After optimization.

Fig.4. Optimization results of the PV pumping system simulation.

The following, we simulated our pumping system with induction motor controlled by DTC-C and using SVM, as is illustrated in Fig. 5. For robustness tests, we take the example of the sunlight (G) fall from 800 to 500 W/m^2.

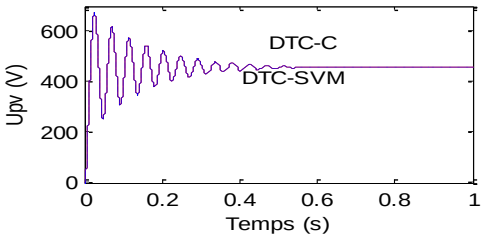

(a) Terminal voltage of PVG Upv (V).

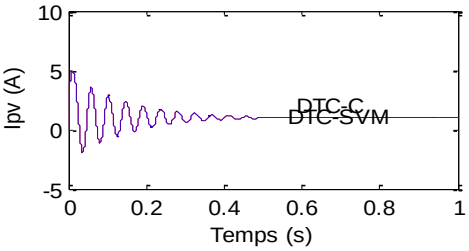

(b) Current debited by PVG Ipv (A)

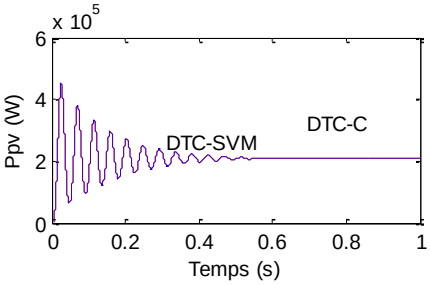

(c) Power debited by the PVG Ppv (W)

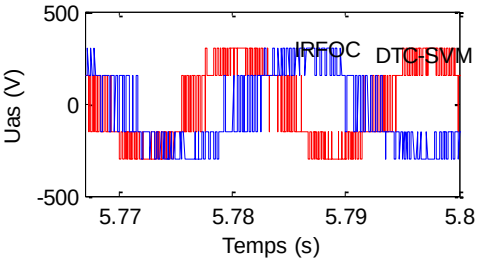

(d) Voltage stator Uas (V)

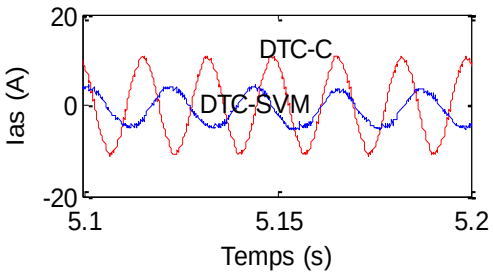

(e) Current of stator Ias (A)

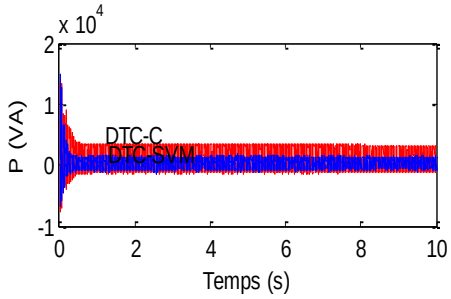

(f) Power consumed by the motor P(VA)

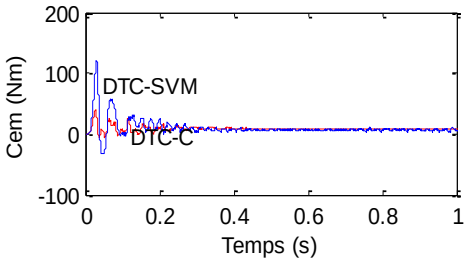

(j) Electromagnetic Torque Tem (Nm)

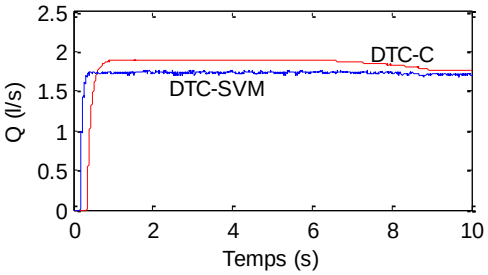

(h) Water flow Q (l/s)

Fig. 5 Comparison between the DTC-C and DTC-SVM applied in the PV pumping system with G varies between 800 and 500 W/m^2.

IX. Interpretation of the Results

The result comparison of the two controls is interpreted by three sides: Transient state; steady state and optimization of the quantity pumped as Following:

A. *Transient state*

Comparing transient concerns, in our case, the settling time of the torque in the case of a transition load and for different values of speed for two cases: DTC-C and DTC-SVM. The results are summarized in Table II. Overall, we find that the settling time of the torque in the DTC-C control is less than that given by the DTC-SVM. This can be explained by the presence of the hysteresis regulator in DTC-C, that causing a delay in the response of torque.

TABLE II
RESPONSES OF TORQUE IN DTC-C AND DTC-SVM WITH HMT = 45M

Control	**DTC-C**	**DTC-SVM**
ω (rad/s)	**settling time of the torque (s)**	
300	0,50	0,27
150	0,42	0,25
100	0,24	0,15

The validation is made for control with speed loop. The aim is to choose the best answer all which gives us a better torque setting for all controls. According to the results, we noted that for some time and for different values of speed (ω = 300, 150 100rad/s), the settling time of the torque in the case of DT-SVM is the most compared to DTC-C. Thanks to this comparison, we chose the results of the DTC-SVM as it provides a better response.

B. *Steady performance*

For a reasonable comparison, the two commands must be the same switching frequency of the inverter. But for the DTC-C, the frequency of the inverter in this technique is variable. This comparison is difficult. We can use a simple means but that does not really solve this problem, consists to modulate the bandwidths regulators hysteresis torque and flux. The switching frequency of the inverter is fixed and the load and speed of rotation. The comparison is made at the level of pulsations of the corrugations of the stator current relative to the reference. The remarks that we can reach is that the rate of torque ripple for DTC-C, namely the torque and stator current in the DTC-SVM differs for different applications load and speed. For example, if we take a speed of ω=100rad/s and T_{load}=10Nm, we can say that our choice fell on the DTC-SVM as it provides a slight reduction in the ripple of both torque and stator current magnitudes. We observe good performance of DTC-SVM control particularly in the stator current and electromagnetic torque, which is considered as an indicator for greater accuracy in setting parameters. In general, the results for the based-vector control are much closer to each other. It should be noted that convergence is significantly faster in the case of DTC-SVM. We also note that the torque oscillations, obtained in the case of DTC-C are significantly larger than in the case of DTC-SVM. The Table III present a comparison of THD in voltage and current in each control.

TABLE III
COMPARISON OF THE THD IN DTC-C AND DTC-SVM.

Control	**DTC-C**	**DTC-SVM**
Electrical size	**THD (%)**	
Iabcs	20,79	29,40
Uabcs	46,35	87,54

C. Optimization of the quantity pumped

The optimization is completed by metering the flow of the pump and the daily amount of water pumped by a numerical integration of the Following equation:

$$q_j = \int_{Tj} Q \cdot dt \tag{7}$$

Where: Q, pump flow. Tj, sunny period of the day.
The method used is that of the Trapezium, and we will then be explicit expression:

$$q_j = 2 \int_{t_1}^{t_n} Q \cdot dt$$

$$q_j = 2\left[Q(t_1) \cdot \frac{\Delta t}{2} + \Delta t \cdot \sum_{i=m_1}^{m_2} Q_i + Q(t_n) \cdot \frac{\Delta t}{2} \right] \tag{8}$$

Where: t_1, Corresponding to the first time the pump that succeeds in defeating the height H_g; t_n, Corresponding time to a maximum illumination; m_1, Index corresponding to time $t=t_1+t$; m_2, Index corresponding to time $t=t_n-\Delta t$; Δt, step of time.
The simulation result of our optimization is shown in Table IV. We have taken G = 1000W/m^2, HMT = 20, 30 and 45m. We have used the DTC-C and DTC-SVM to control the induction motor with P_m=1,5KW ω=150rad/s.

TABLE IV
VARIATION OF THE DAILY AMOUNT OF WATER PUMPED ACCORDING TO THE HMT.

Control	**DTC-C**			**DTC-SVM**		
HMT[m]	20	20	20	20	20	20
Q[l/s]	2,88	2,50	1,95	3,28	2,85	2,18

X. CONCLUSION

Throughout this study, we have developed a numerical simulation for the PV water pumping system and its control structure. We applied the DTC-C and DTC-SVM. Finally we noticed that the DTC-SVM, more than its simplicity, provides a quick and accurate response of the stator flux and the electromagnetic torque. This allows a fairly rapid response of the pumping system. Thus, as we saw in the robustness tests the system remains stable even when the decrease in sunlight which leads to improved robustness with respect to parameter variations. And it is well suited for techno-economic needs of the order of a PV water pumping system.

REFERENCES

[1] A.G. Aberle, S.R. Wenham, M.A. Green. "A new Method for Accurate Measurements of the Lumped Series Resistance of Solar Cells". *Proceedings of the 23rd IEEE Photovoltaic Specialists Conference*: 113-139, 1993.

[2] D. Rekioua, E. Matagne "Optimization of Photovoltaic Power Systems Modelization, Simulation and Control". book_978-1-4471-2403-0.pdf

[3] D. Prasad, BP. Panigrahi, S. SenGupta, "Digital simulation and hardware implementation of a simple scheme for direct torque control of induction motor", *Energy Conversion and Management*, 49(4), pp. 687-697, 2008.

[4] M. Chergui, M. Bourahla, "Application of The calculated PWM technique in the photovoltaic pumping system", *Environment Friendly Energies and Applications, 2nd International Symposium on Digital Object Identifier*, paper 10.1109/EFEA.2012.6294052, p. 341.

[5] R. Kennel, EE. El-kholy, S. Mahmoud, A. El-refaei, F. Elkady, "Improved direct control for induction motor drives with rapid prototyping system", *Energy Conversion and Management*, 47(13), pp. 1999–2010, 2006.

[6] R. Krishnan, A.S. Bharadwaj, "A review of parameter sensitivity and adaptation in indirect vector controlled induction motor drive", *IEEE Trans. Power. Elect*, 6(4), pp. 695-70, 1991.

[7] A. Mokeddem, A. Midoun, D. Kadri, S. Hiadsi, A. Raja Iftikhar, "Performance of a directly-coupled PV water pumping system". *Energy Conversion and Management*, 52(10), pp. 3089–95, 2011.

[8] B. Parida, S. Iniyan, R.A. Goic, "Review of solar photovoltaic technologies". *Renew Sust Energy Rev*, 15(3), pp. 1625–36, 2011.

[9] L. Antonio, H. Steven, *Handbook of Photovoltaic Science and Engineering*. John Wiley and Sons. ISBN 0-471-49196-9, 2003.

[10] B. Belgacem., "Performance of submersible PV water pumping systems in Tunisia". *Energy for Sustainable Development*, 16(4), pp. 415–420, 2012.

[11] C.H. Henry. "Limiting efficiencies of ideal single and multiple energy gap terrestrial solar cells". *J. Appl. Phys*. 51: 4494.1980.

[12] W. Cheng-Hsiao, W. Richard. "Limiting efficiencies for multiple energy-gap quantum devices". J. Appl. Phys. 54: 6721. 1983.

[13] H. Sher, K.E. Addoweesh, "Micro-inverters-Promising solutions in solar photovoltaic". *Energy for Sustainable Development*. 16(4), pp. 389–400, 2012.

[14] J.M. Enrique, E. Dura´n, M. Sidrach-de-Cardona, J. M. Andu´jar, "Theoretical assessment of the maximum power point tracking efficiency of photovoltaic facilities with different converter topologies". Solar Energy. Vol. 81, pp. 31–38, 2007.

[15] D. P. Hohm, M. E. Ropp, "Comparative study of maximum power point tracking algorithms", *Progress in photovoltaic, research and applications*. Vol.11, No. 1, pp. 47-62, 2003.

[16] C. Hua, J. Lin, "A modified tracking algorithm for maximum power tracking of solar array", *Energy conversion and Management*, Vol. 45, pp. 911-925, April 2004.

[17] M. Chergui, M. Bourahla, "Application of the DTC control in the photovoltaic pumping system", *Energy Conversion and Management*, 65, pp. 655–662, Jan.2013.

[18] MN. Eskander, M.Z. Aziza, "A Maximum Efficiency-Photovoltaic-Induction motor pumping system", *Renewable Energy*, 10(1), pp. 53–60, 1997.

[19] D Prasad, BP Panigrahi, S SenGupta. "Digital simulation and hardware implementation of a simple scheme for direct torque control of induction motor". *Energy Conversion and Management*. 49(4): 687-697. 2008.